Int. J. Heat Mass Transfer. Vol. 37, No. 2, pp. 195–206, 1994
Printed in Great Britain

0017–9310/94 $6.00 + 0.00

On natural convection in vertical porous enclosures due to opposing fluxes of heat and mass prescribed at the vertical walls

FARID ALAVYOON,† YOSHIO MASUDA and SHIGEO KIMURA
Government Industrial Research Institute, Tohoku, Agency of Industrial Science and Technology, Ministry of International Trade and Industry, Nigatake, 4-2-1, Miyagino-Ku, Sendai, 983, Japan

(*Received* 1 *March* 1993 *and in final form* 6 *August* 1993)

Abstract—A two-dimensional mathematical model based on Darcy's law with Boussinesq approximation has been used to study double-diffusive natural convection in a rectangular fluid-saturated vertical porous enclosure subject to opposing and horizontal gradients of heat and solute. Results are presented for $50 \leqslant R_c \leqslant 250$, $0.01 \leqslant N \leqslant 10$, $10 \leqslant Le \leqslant 40$ and $1 \leqslant A \leqslant 10$, where R_c, N, Le and A correspond to the solutal Rayleigh–Darcy number, inverse of buoyancy ratio, Lewis number and enclosure aspect ratio, respectively. The numerical integration of the full problem reveals that for sufficiently large R_c, Le and A, there is a domain of N in which one obtains oscillating convection. Outside this domain, the solution approaches steady-state convection, for which analytical solutions are developed and presented. The agreement between the analytical and the numerical solutions is shown to be satisfactory.

1. INTRODUCTION

NATURAL convection due to spatial variations of fluid density is of fundamental importance in many natural and industrial problems. The variation of fluid density can be due to nonuniform distribution of temperature and/or solute concentration. Some examples of heat and/or solute transfer by natural convection can be found in: oceanography, geophysics, astrophysics, metallurgy and electrochemistry. Most of the reported surveys on natural convection deal with cases in which the buoyancy forces are due to the variations of only temperature or concentration. The interest of research in the case of flow due to variations of both temperature and concentration has surged during recent years. Such phenomena are usually referred to as thermohaline, double diffusive or combined heat and mass transfer natural convection. Since heat and solute diffuse at widely different rates, double diffusive phenomena often exhibit special features, such as fingering and layering, that lack counterparts in single-component cases, see refs. [1–3].

In the present paper we report a theoretical study of double diffusive natural convection in a fluid-saturated rectangular porous enclosure. Fluid motion is caused by buoyancy forces which, in turn, stem from constant and opposing gradients of temperature and concentration of a dissolved substance prescribed on the vertical walls of the enclosure. Of primary relevance to the present work is the paper by Trevisan and Bejan [4] in which the authors reported numerical and analytical results for a fluid-saturated rectangular porous enclosure subject to constant gradients of temperature and concentration at the vertical walls. Based on the results of an earlier work by Bejan [5], the authors developed an analytical boundary layer solution to the problem, which proved to be valid only for the case of $Le = 1$. Instead, for $Le > 1$, an analytical similarity solution was presented in the heat-driven limit. In a recent paper, Alavyoon [6] further developed the solution given in the first part of ref. [4] to account for the case of $Le > 1$ in a porous cavity with natural convection due to cooperative buoyancy forces. The present paper reports the results obtained through an extension to opposing buoyancy forces of the analytical model given in ref. [6]. In addition, the phenomenon of oscillating convection, which is observed for certain parameter ranges, is discussed. The occurrence of oscillating convection in porous media, both for single-component and for double-diffusive cases, has been previously observed and reported by several authors, see e.g. refs. [7–11]. In these papers, the authors consider natural convection in horizontally placed rectangular porous enclosures subject to vertical gradients of heat or/and solute. To the best of our knowledge, oscillating convection in vertical porous layers subject to horizontal gradients of heat and solute have not been reported prior to the present work.

For an overview of previous work on double diffusive natural convection in porous media see refs. [1, 12].

† Author to whom correspondence should be addressed. Present address: Vattenfall Utveckling AB, S-810 70 Älvkarleby, Sweden.

NOMENCLATURE

A	aspect ratio
br	buoyancy ratio, $\beta\Lambda^{(c)}/\alpha\Lambda^{(T)}$
D	solute diffusivity
g	acceleration of gravity
$2h$	enclosure width
$2H$	enclosure height
k	permeability
Le	Lewis number
N	inverse of buoyancy ratio, $1/br$
Nu	Nusselt number
P	pressure
R	Rayleigh–Darcy number
S	vertical gradient
Sh	Sherwood number
t	time
$\mathbf{u}$	velocity vector, (u, v)
x	horizontal coordinate
y	vertical coordinate.

Greek symbols

α	coefficient of thermal expansion
β	coefficient of concentration expansion
ε	porosity
θ	nondimensional concentration variation
ϑ	horizontal profile
κ	thermal diffusivity
Λ	horizontal gradient prescribed on the side wall
ν	kinematic viscosity
ρ	density
σ	heat capacity ratio
ϕ	nondimensional temperature variation.

Subscripts and superscripts

c	solutal
T	thermal
0	initial.

2. PROBLEM STATEMENT

Consider a two-dimensional vertical enclosure filled with a homogeneous fluid-saturated porous medium of height $2H$ and width $2h$. The fluid is initially uniform and at rest. The top and the bottom walls of the enclosure are insulated. Constant and opposing fluxes of heat and solute are prescribed on the vertical walls. In the present analysis, the conservation of momentum, volume, solute concentration and heat is modelled by the following system of dimensionless equations [6]

$$\mathbf{u} = -\nabla P - R_c(\theta - N\phi)\mathbf{e}_y \tag{1}$$

$$\nabla \cdot \mathbf{u} = 0 \tag{2}$$

$$\varepsilon\frac{\partial\theta}{\partial t} + \mathbf{u}\cdot\nabla\theta = \nabla^2\theta \tag{3}$$

$$\sigma\frac{\partial\phi}{\partial t} + \mathbf{u}\cdot\nabla\phi = Le\nabla^2\phi \tag{4}$$

where

$$R_c = \frac{kg\beta\Lambda^{(c)}h^2}{\nu D}, \quad N = \frac{\alpha\Lambda^{(T)}}{\beta\Lambda^{(c)}}$$

and

$$Le = \frac{\kappa}{D}.$$

The boundary and initial conditions are

$$\frac{\partial\theta}{\partial y} = 0, \quad \frac{\partial\phi}{\partial y} = 0 \quad \text{and } v = 0 \text{ at } |y| = A \tag{5}$$

$$\frac{\partial\theta}{\partial x} = -1, \quad \frac{\partial\phi}{\partial x} = -1 \quad \text{and } u = 0 \text{ at } |x| = 1 \tag{6}$$

$$\theta(x, y, 0) = 0, \quad \phi(x, y, 0) = 0 \text{ and } \mathbf{u}(x, y, 0) = 0 \tag{7}$$

where $A = H/h$, see Fig. 1.

The boundary condition (6) corresponds to influx of heat and solute at $x = -1$ and the opposite at $x = 1$.

3. NUMERICAL METHOD

The time-dependent evolution of the velocity, concentration and temperature fields is numerically com-

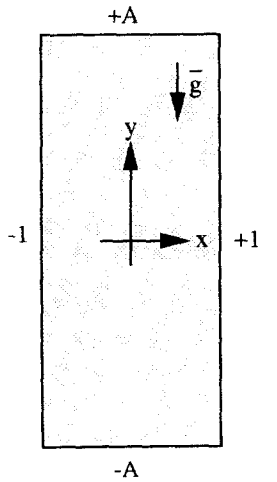

FIG. 1. The geometry of the porous enclosure.

puted by using finite differences. The equations and boundary conditions are discretized on a rectangular mesh with uniform spacing in each coordinate direction. The pressure gradient term in equation (1) is eliminated by using its stream function version. The convective terms in equations (3) and (4) are evaluated at the last time step for which the solution is known. The resulting numerical scheme is first-order accurate in time and second-order accurate in space. The discretized equations and boundary conditions define three linear systems of algebraic equations that are solved at each time step by the method of conjugate gradients in order to determine the values of stream function, concentration and temperature at each grid point. For more details see ref. [6].

4. ANALYTICAL SOLUTION FOR THE STEADY STATE

4.1. *General*

If the enclosure is sufficiently high for end effects to be negligible except for in the vicinity of the horizontal boundaries, one can assume that the steady-state solution outside the end regions has the following form [6]

$$\mathbf{u} = v(x)\mathbf{e}_y \tag{8}$$

$$\theta = S_c y + \vartheta_c(x) \tag{9}$$

$$\phi = S_T y + \vartheta_T(x) \tag{10}$$

$$\nabla P = \{\Pi_y - R_c(S_c - NS_T)y\}\mathbf{e}_y \tag{11}$$

where S_c, S_T and Π_y are unknown constants, and $v(x)$, $\vartheta_c(x)$ and $\vartheta_T(x)$ are unknown functions to be determined.

Introducing relationships (8)–(11) into equations (1), (3) and (4) and boundary condition (6), one obtains a linear system of second-order ordinary differential equations

$$v(x) = -\Pi_y - R_c\vartheta_c(x) + R_cN\vartheta_T(x) \tag{12}$$

$$v(x)S_c = \frac{d^2\vartheta_c}{dx^2} \tag{13}$$

$$v(x)S_T = Le\frac{d^2\vartheta_T}{dx^2} \tag{14}$$

$$\frac{d\vartheta_c}{dx} = -1 \quad \text{at } x = \pm 1 \tag{15}$$

$$\frac{d\vartheta_T}{dx} = -1 \quad \text{at } x = \pm 1 \tag{16}$$

which define the mathematical problem to be solved for determining $v(x)$, $\vartheta_c(x)$ and $\vartheta_T(x)$ in terms of the yet unknown constants S_c, S_T and Π_y and two integration constants. In order to determine these five unknowns, five integral conditions have to be imposed on the solution. These conditions read [6]

1. Conservation of volume:

$$\int_{-1}^{+1} v(x)\,dx = 0 \tag{17}$$

2. Conservation of total mass:

$$\int_{-A}^{+A}\int_{-1}^{+1} \varepsilon\theta\,dx\,dy = 2A\varepsilon\int_{-1}^{+1}\vartheta_c(x)\,dx = 0 \tag{18}$$

3. Conservation of total enthalpy:

$$\int_{-A}^{+A}\int_{-1}^{+1} \sigma\phi\,dx\,dy = 2A\sigma\int_{-1}^{+1}\vartheta_T(x)\,dx = 0 \tag{19}$$

4. Balance between convective and diffusive transports of solute at arbitrary horizontal cross-section:

$$\int_{-1}^{+1}(\mathbf{u}\theta - \nabla\theta)\cdot\mathbf{e}_y\,dx = \int_{-1}^{+1} v\vartheta_c\,dx - 2S_c = 0 \tag{20}$$

5. Balance between convective and diffusive transports of enthalpy at arbitrary horizontal cross-section:

$$\int_{-1}^{+1}(\mathbf{u}\phi - Le\,\nabla\phi)\cdot\mathbf{e}_y\,dx = \int_{-1}^{+1} v\vartheta_T\,dx - 2\,Le\,S_T = 0. \tag{21}$$

The mathematical problem defined by equations (12)–(14) and the boundary and integral conditions (15)–(21) is a well-posed problem which can be solved rather easily. Below follows the solving procedure and the different possible solutions to this problem.

4.2. *Solution procedure*

The temperature profile ϑ_T can be given in terms of the concentration profile ϑ_c by combining equations (13) and (14), which gives

$$\frac{d^2\vartheta_T}{dx^2} = \frac{S_T}{Le\,S_c}\frac{d^2\vartheta_c}{dx^2}$$

and thereafter integrating twice, and invoking the boundary conditions (15) and (16) and the integral conditions (18) and (19), which yields

$$\vartheta_T = \frac{S_T}{Le\,S_c}\vartheta_c + \left(\frac{S_T}{Le\,S_c} - 1\right)x. \tag{22}$$

The velocity profile $v(x)$ can be expressed in terms of ϑ_c by substituting (22) into (12)

$$v(x) = -\Pi_y + R_c\left(\frac{NS_T}{Le\,S_c} - 1\right)\vartheta_c(x) + R_c\left(\frac{N\,S_T}{Le\,S_c} - N\right)x. \tag{23}$$

The value of the constant Π_y can be determined by applying the integral conditions (17) and (18) to formula (23), from which one obtains $\Pi_y = 0$. Finally, the second-order linear ordinary differential equation

$$\frac{d^2\vartheta_c}{dx^2} - (R_T S_T - R_c S_c)\vartheta_c = (R_T S_T - N R_c S_c)x \quad (24)$$

where $R_T = R_c(N/Le)$, can be obtained for ϑ_c by inserting (23) into equation (13) and rearranging the terms. For convenience, we introduce the notations

$$\Omega = \sqrt{(R_T S_T - R_c S_c)}$$

and

$$B = \frac{R_T S_T - N R_c S_c}{R_T S_T - R_c S_c}.$$

A complication which arises here compared to the case of cooperating fluxes of heat and solute [6] is that the parameter Ω, depending on the values of R_c, N and Le, can become real, imaginary or zero. The solutions for these three cases are given in the next subsections.

4.2.1. $R_T S_T - R_c S_c > 0$ (Ω *real*). Assume that the values of the input parameters R_c, Le and N, are such that the final results satisfy the condition $R_T S_T - R_c S_c > 0$, i.e. Ω is real. In terms of the yet unknown constants S_c, S_T, Ω and B, the solution to the equation (24) reads

$$\vartheta_c(x) = \frac{B-1}{\Omega \cosh(\Omega)} \sinh(\Omega x) - Bx. \quad (25)$$

The expression for ϑ_T is given by (22) and the velocity profile can be computed by substituting (26) into equation (13)

$$v(x) = \frac{\Omega(B-1)}{S_c \cosh(\Omega)} \sinh(\Omega x). \quad (26)$$

It remains to determine the values of S_c and S_T. Substituting (22), (25) and (26) into the integral conditions (20) and (21) gives the nonlinear and coupled system of algebraic equations

$$S_c^2 - \frac{(B-1)^2}{1+\cosh(2\Omega)}\left(\frac{\sinh(2\Omega)}{2\Omega} - 1\right) + B(B-1)\left(1 - \frac{\tanh(\Omega)}{\Omega}\right) = 0 \quad (27)$$

$$\left(1 - \frac{1}{Le^2}\right)S_T - \left(\frac{1}{Le}\frac{S_T}{S_c} - 1\right) \times \left(1 - \frac{\tanh(\Omega)}{\Omega}\right)\frac{B-1}{Le\,S_c} = 0 \quad (28)$$

from which S_c and S_T can be determined for given values of R_c, N and Le. For the general case, equations (27) and (28) have to be solved numerically, e.g. by Newton–Raphson's method. However, this is a much easier task than numerically solving the full set of equations given in (1)–(7).

Once S_c and S_T, and thereby B and Ω, are known, the values of the overall Sherwood and Nusselt numbers can be computed from

$$Sh = \frac{2A}{\frac{1}{2}\int_{-A}^{+A}\{(\theta)_{x=-1} - (\theta)_{x=+1}\}\,dy} \quad (29)$$

$$Nu = \frac{2A}{\frac{1}{2}\int_{-A}^{+A}\{(\phi)_{x=-1} - (\phi)_{x=+1}\}\,dy} \quad (30)$$

which in view of (9), (10), (22) and (25) reduce to

$$Sh = \frac{2}{\vartheta_c(-1) - \vartheta_c(+1)} = \left[B - (B-1)\frac{\tanh(\Omega)}{\Omega}\right]^{-1} \quad (31)$$

$$Nu = \left[\frac{S_T}{Le\,S_c}\frac{1}{Sh} + 1 - \frac{S_T}{Le\,S_c}\right]^{-1}. \quad (32)$$

4.2.2. $R_T S_T - R_c S_c < 0$ (Ω *imaginary*). Assume that the values of the input parameters are such that Ω becomes imaginary. We can still use the solution given in the previous subsection by simply replacing Ω with $i\omega$, where $i = \sqrt{(-1)}$ and $\omega = \sqrt{(R_c S_c - R_T S_T)}$ (real). One thus obtains

$$v(x) = -\frac{\omega(B-1)}{S_c \cos(\omega)} \sin(\omega x) \quad (33)$$

for the velocity profile and

$$\vartheta_c(x) = \frac{B-1}{\omega \cos(\omega)} \sin(\omega x) - Bx \quad (34)$$

for the concentration profile. The temperature profile ϑ_T is given by (22). The values of S_c and S_T can be determined by numerically solving the following equations

$$S_c^2 - \frac{(B-1)^2}{1+\cos(2\omega)}\left(\frac{\sin(2\omega)}{2\omega} - 1\right) + B(B-1)\left(1 - \frac{\tan(\omega)}{\omega}\right) = 0 \quad (35)$$

$$\left(1 - \frac{1}{Le^2}\right)S_T - \left(\frac{1}{Le}\frac{S_T}{S_c} - 1\right) \times \left(1 - \frac{\tan(\omega)}{\omega}\right)\frac{B-1}{Le\,S_c} = 0. \quad (36)$$

Extensive numerical calculations show that in some cases, for given values of R_c, Le and N, the equation system (35) and (36) may have more than one solution. Only the solution that fulfils the conditions $S_c - N S_T < 0$ and $\omega < \pi$ can agree with the fully numerical computations. Note that the first of the aforementioned conditions requires that the average density of the fluid across every horizontal cross section should decrease upwards.

The Sherwood number can be computed from

$$Sh = \left[B - (B-1)\frac{\tan(\omega)}{\omega}\right]^{-1} \quad (37)$$

and the Nusselt number from expression (32).

An important matter which now remains to be resolved is the question of how, for given values of R_c, Le and N, one can anticipate whether or not Ω becomes imaginary. In order to answer this question, one has first to find out for what values of the input parameters, Ω becomes zero. This matter is considered in the next subsection. The domain of validity of the analytical solutions will be discussed more in Section 5.

4.2.3. $R_T S_T - R_c S_c = 0$ ($\Omega = 0$). In this subsection it is assumed that R_c and Le are known, and N is determined so that Ω becomes zero. If $\Omega = 0$ then, in view of the definition of Ω, S_T can be given in terms of S_c by the relationship

$$S_T = \frac{Le}{N} S_c. \tag{38}$$

The solution to (24) then reads

$$\vartheta_c(x) = \frac{1-N}{2} R_c S_c \left(\frac{x^3}{3} - x\right) - x. \tag{39}$$

Substitute (39) into (13) to obtain the velocity profile

$$v(x) = (1-N) R_c x. \tag{40}$$

In view of (38), expression (22) for the temperature field reduces to

$$\vartheta_T(x) = \frac{1}{N} \vartheta_c(x) + \left(\frac{1}{N} - 1\right) x. \tag{41}$$

Next, substituting (39) and (40) into the integral condition (20) gives S_c, and thereby according to (38) also S_T, in terms of N

$$S_c = \frac{(N-1)^2}{3(Le^2-1)} R_c. \tag{42}$$

Finally, substituting (38)–(42) into the integral condition (21) yields the equation

$$\tfrac{2}{15}(N-1)^3 R_c^2 + N - Le^2 = 0 \tag{43}$$

which has to be satisfied in order to get a solution for which $\Omega = 0$. Equation (43) is a third degree polynomial in N which has only one real root. For given values of R_c and Le, equation (43) can be easily solved by, e.g., graphic or numerical methods. However, for $Le > 2$ and $R_c > 10$, which are not so inconveniently restrictive conditions, the only real root of equation (43) can be accurately estimated by the expression

$$N \approx 1 + \left(\frac{15}{2}\right)^{1/3} \left(\frac{Le}{R_c}\right)^{2/3}. \tag{44}$$

5. RESULTS AND DISCUSSION

A large number of numerical computations have been carried out to investigate the time-dependent and the steady-state behaviors of the system under consideration. The variations of the analytically and the numerically computed values of Sh and Nu vs R_c ($10 \leqslant R_c \leqslant 1000$), for $Le = 25$, $N = 5$ and $A = 20$, vs Le ($1.5 \leqslant Le \leqslant 10$), for $R_c = 250$, $N = 0.5$ and $A = 20$, and vs A ($1 \leqslant A \leqslant 5$), for $R_c = 1000$, $Le = 10$ and $N = 2$, have already been reported in ref. [13]. In the present analysis, emphasis is put on how the solution evolves when N is continuously varied. With the main goals of validating the analytical solutions, delineating their domains of validity and reporting the possibility of occurrence of unsteady oscillating convection, a representative set of the results are selected and shown in Figs. 2–14 and in Table 1. Since the aspect ratio of the cavity proves to play a crucial role in the qualitative and the quantitative features of the solution, first the case of high aspect ratios ($A \geqslant 2.5$ in this paper) and then the case of moderate values of the aspect ratio ($1 \leqslant A < 2.5$ in this paper) will be discussed.

5.1. *The case of high aspect ratios* ($A \geqslant 2.5$)

The numerical computations show that for sufficiently large values of R_c and Le, there exists a lower (N_{min}) and an upper (N_{max}) limit for N such that for $N \leqslant N_{min}$ or $N \geqslant N_{max}$, the solution goes towards

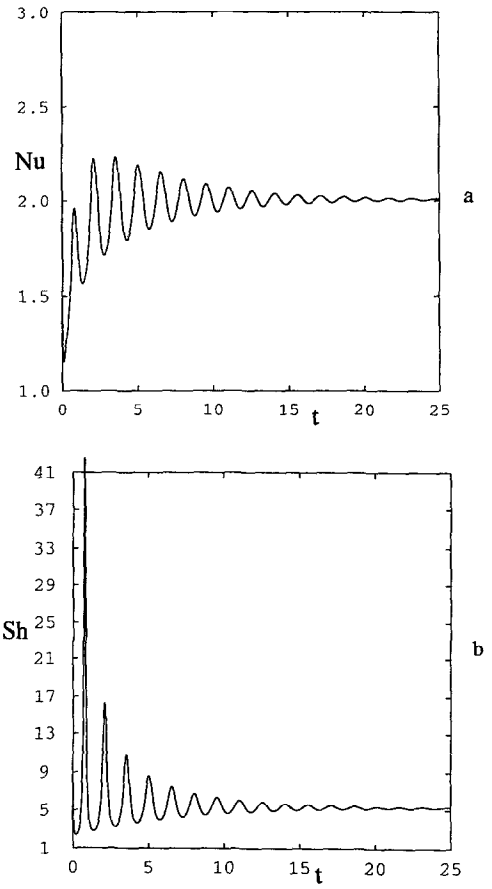

FIG. 2. $R_c = 100$, $Le = 10$, $N = 1$ and $A = 5$, (a) Nusselt number vs time, and (b) Sherwood number vs time.

Table 1. Parameter ranges for which oscillating convection occurs

Le	N_{min}	N_{max}
	$R_c = 100$ and $A = 10$	
10	0.60	0.90
20	0.55	0.85
30	0.55	0.80
40	0.55	0.80
	$R_c = 100$ and $A = 5$	
10	0.60	0.80
20	0.60	0.75
30	0.55	0.75
40	0.55	0.70
	$R_c = 100$ and $A = 3$	
10	0.60	0.60
20	0.55	0.65
30	0.55	0.65
40	0.50	0.65
	$R_c = 250$ and $A = 5$	
10	0.60	1.20
20	0.50	1.20
30	0.50	1.0
40	0.50	1.0

steady state while for $N_{min} \leqslant N \leqslant N_{max}$ the solution evolves towards a permanently oscillating state of convection, see Figs. 2 and 3. N_{min} and N_{max} are determined numerically, with an error of $|\Delta N| \approx 0.05$, for various values of the input parameters R_c, Le and A and given in Table 1. Note that for $N = 1$

$$\theta = \phi = -x \quad \text{and} \quad \mathbf{u} = 0$$

is an exact solution to the equations (1)–(4) subject to the boundary conditions (5) and (6). According to this solution $Sh = Nu = 1$, which means that heat and mass transfer is in the purely diffusive regime. However, Fig. 2 shows that the numerical integration of the full system of equations leads to a different solution in which convection plays a dominant role in the transfer of heat and mass. The oscillating motion, which is a consequence of the double-diffusive feature of the present problem, is observed in cases where the contribution of the gradients of temperature and solute concentration to buoyancy are of comparable magnitude. Streamlines and contours of concentration, temperature and density during a cycle are given in Figs. 4–7. Generally speaking, one can distinguish two categories of streamlines in Fig. 4: (A) those nearest to the solid boundaries and covering the whole height of the enclosure (Figs. 4(a)–(j)), and (B) those in the upper and lower halfs of the core region, covering at most half of the enclosure height (Figs. 4(c)–(e)). The streamlines of category A are present in the flow field all the time while those of category B appear and disappear periodically. Note that the fluid motion on all of these streamlines is in the clockwise direction. According to Fig. 4, following a decrease in the magnitude of velocity, Figs. 4(a) and (b), the unicellular pattern of streamlines (consisting of streamlines of category A) tends to develop into a bicellular pattern, Figs. 4(c)–(e). This development starts when two convective cells (streamlines of category B) appear in the upper and lower core regions. The motion of these two convective cells reduces the vertical stratification of the density field (Figs. 7(c)–(e)), and as a result weakens the blocking effect of stratification on the vertical motion of the fluid, thus allowing the convective cells to extend their vertical span towards the middle of the enclosure. In Figs. 4(c)–(e), the horizontal motion of the fluid near the middle of the enclosure in the lower (upper) part of the upper (lower) convective cells is from right to left (left to right). Therefore, upon reaching the middle of the enclosure, the upper and lower convective cells in Figs. 4(c)–(e) gradually merge, see Figs. 4(e) and (f), and the horizontal motion near the half-height of the enclosure disappears, filling the whole enclosure with the streamlines of category A. Thereafter, the density field becomes progressively more stratified, Figs. 7(f)–(j) and 7(a), (b), the flow velocity diminishes, and the cycle is repeated. Note that according to Fig. 5, the concentration field (the component with low diffusivity) goes through dramatic changes during a period

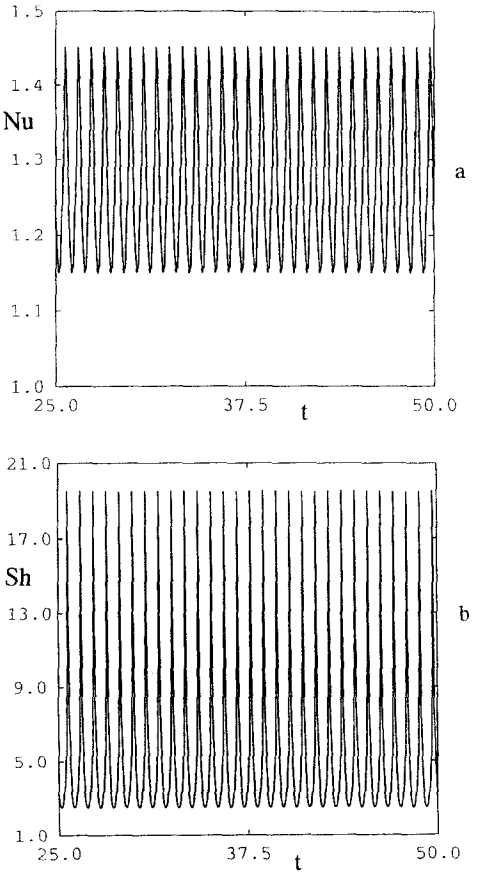

FIG. 3. $R_c = 100$, $Le = 20$, $N = 0.6$ and $A = 5$, (a) Nusselt number vs time, and (b) Sherwood number vs time.

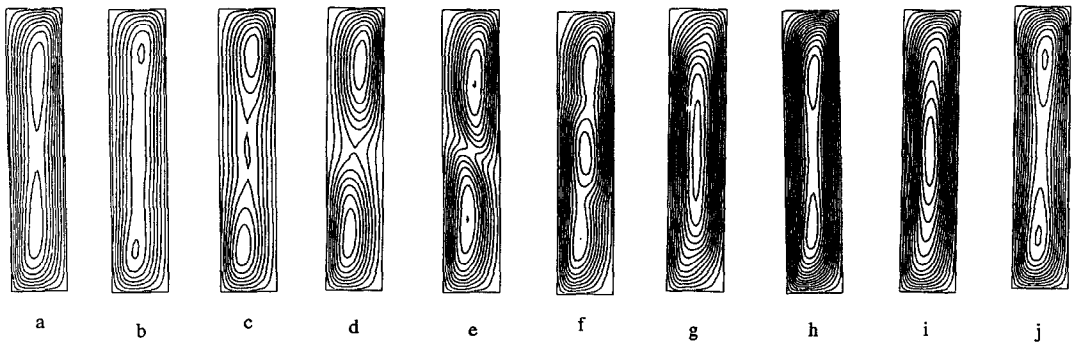

FIG. 4. Contour lines of stream function ψ during a period of oscillations. $R_c = 100$, $Le = 20$, $N = 0.6$, $A = 5.0$, $\Delta\psi = 2.0$, ψ increasing from the boundaries inwards (clockwise flow direction). (a) $t = 36.344$, $0.0 \leqslant \psi \leqslant 15.0$, (b) $t = 36.431$, $0.0 \leqslant \psi \leqslant 13.0$, (c) $t = 36.518$, $0.0 \leqslant \psi \leqslant 13.0$, (d) $t = 36.605$, $0.0 \leqslant \psi \leqslant 15.0$, (e) $t = 36.692$, $0.0 \leqslant \psi \leqslant 19.0$, (f) $t = 36.779$, $0.0 \leqslant \psi \leqslant 21.0$, (g) $t = 36.886$, $0.0 \leqslant \psi \leqslant 25.0$, (h) $t = 36.953$, $0.0 \leqslant \psi \leqslant 27.0$, (i) $t = 37.040$, $0.0 \leqslant \psi \leqslant 27.0$ and (j) $t = 37.127$, $0.0 \leqslant \psi \leqslant 21.0$.

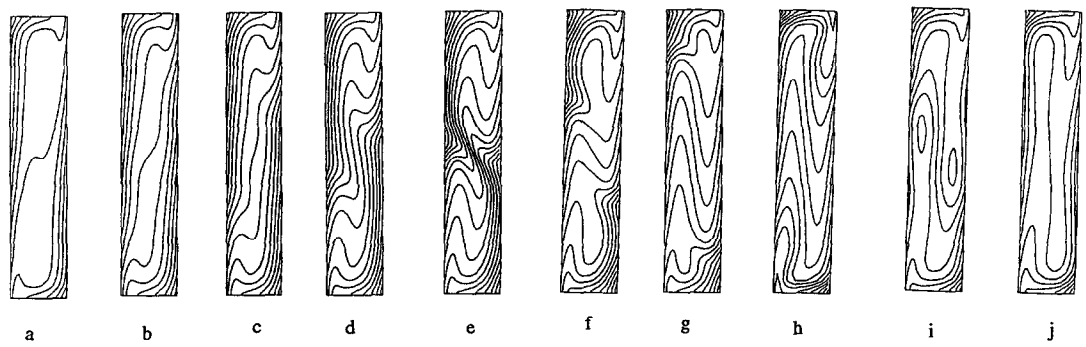

FIG. 5. Contour lines of concentration θ during a period of oscillations. $R_c = 100$, $Le = 20$, $N = 0.6$, $A = 5.0$, $\Delta\theta = 0.1$, θ increasing upwards. (a) $t = 36.344$, $-0.6 \leqslant \theta \leqslant 0.6$, (b) $t = 36.431$, $-0.7 \leqslant \theta \leqslant 0.7$, (c) $t = 36.518$, $-0.8 \leqslant \theta \leqslant 0.8$, (d) $t = 36.605$, $-0.9 \leqslant \theta \leqslant 0.9$, (e) $t = 36.692$, $-1.0 \leqslant \theta \leqslant 1.0$, (f) $t = 36.779$, $-1.0 \leqslant \theta \leqslant 1.0$, (g) $t = 36.886$, $-1.0 \leqslant \theta \leqslant 1.0$, (h) $t = 36.953$, $-0.9 \leqslant \theta \leqslant 0.9$, (i) $t = 37.040$, $-0.7 \leqslant \theta \leqslant 0.7$ and (j) $t = 37.127$, $-0.7 \leqslant \theta \leqslant 0.7$.

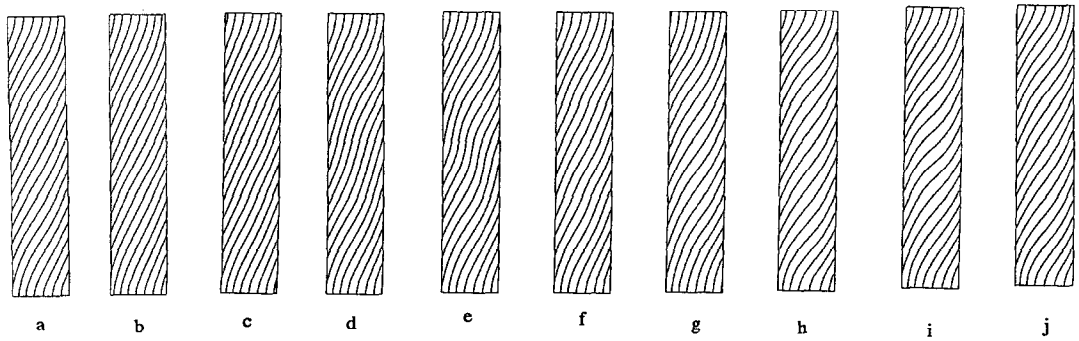

FIG. 6. Contour lines of temperature ϕ during a period of oscillations. $R_c = 100$, $Le = 20$, $N = 0.6$, $A = 5.0$, $\Delta\phi = 0.25$, ϕ increasing upwards. (a) $t = 36.344$, $-2.5 \leqslant \phi \leqslant 2.5$, (b) $t = 36.431$, $-2.5 \leqslant \phi \leqslant 2.5$, (c) $t = 36.518$, $-2.5 \leqslant \phi \leqslant 2.5$, (d) $t = 36.605$, $-2.5 \leqslant \phi \leqslant 2.5$, (e) $t = 36.692$, $-2.25 \leqslant \phi \leqslant 2.25$, (f) $t = 36.779$, $-2.25 \leqslant \phi \leqslant 2.25$, (g) $t = 36.886$, $-2.5 \leqslant \phi \leqslant 2.5$, (h) $t = 36.953$, $-2.5 \leqslant \phi \leqslant 2.5$, (i) $t = 37.040$, $-2.5 \leqslant \phi \leqslant 2.5$ and (j) $t = 37.127$, $-2.75 \leqslant \phi \leqslant 2.75$.

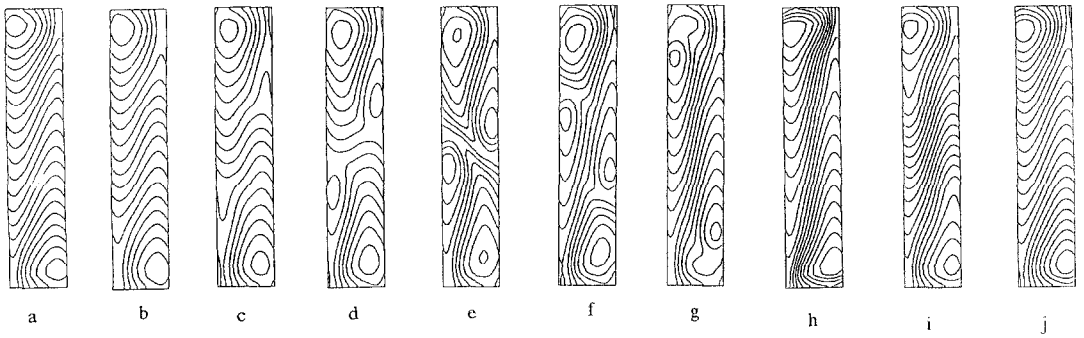

FIG. 7. Contour lines of density $\rho = \theta - N\phi$ during a period of oscillations. $R_c = 100$, $Le = 20$, $N = 0.6$, $A = 5.0$, $\Delta\rho = 0.1$, ρ increasing downwards. (a) $t = 36.344$, $-1.1 \leqslant \rho \leqslant 1.1$, (b) $t = 36.431$, $-0.9 \leqslant \rho \leqslant 0.9$, (c) $t = 36.518$, $-0.8 \leqslant \rho \leqslant 0.8$, (d) $t = 36.605$, $-0.7 \leqslant \rho \leqslant 0.7$, (e) $t = 36.692$, $-0.7 \leqslant \rho \leqslant 0.7$, (f) $t = 36.779$, $-0.7 \leqslant \rho \leqslant 0.7$, (g) $t = 36.886$, $-0.8 \leqslant \rho \leqslant 0.8$, (h) $t = 36.953$, $-1.0 \leqslant \rho \leqslant 1.0$, (i) $t = 37.040$, $-1.1 \leqslant \rho \leqslant 1.1$ and (j) $t = 37.127$, $-1.2 \leqslant \rho \leqslant 1.2$.

of oscillation. The temperature field (the component with high diffusivity) on the other hand, is only weakly distorted. In view of the changes that the density field goes through in Fig. 7, one may infer that the destabilizing influence of horizontal density gradients on the flow field is responsible for the occurrence of oscillating convection. For larger values of N ($N > N_{max}$), this destabilizing influence is subdued by the stabilizing influence of the vertical stratification of density and the oscillations are damped progressively until a steady state of convection is established. For the time-dependent development of the contour lines of the cases which lead to steady state see ref. [13].

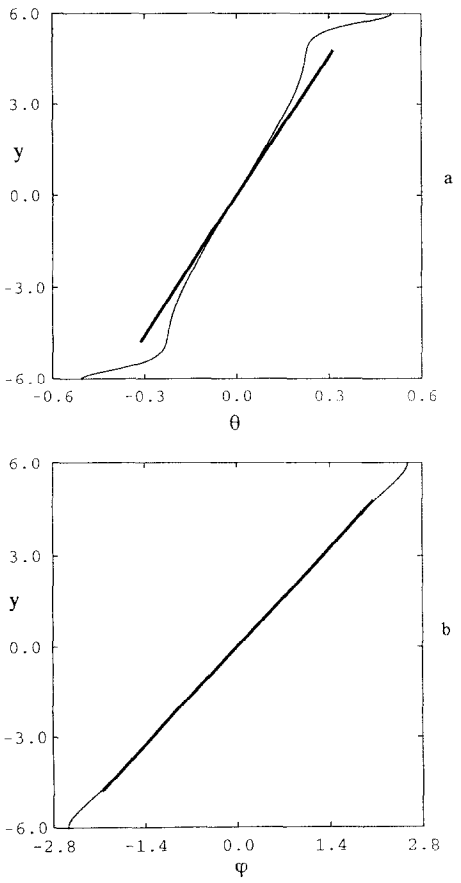

FIG. 8. Comparison between the fully numerical (thin line) and the analytical (iω) solutions (thick line) for $R_c = 100$, $Le = 10$, $N = 1.1$, $A = 6$ and $x = 0$, (a) concentration profile, and (b) temperature profile.

The fully numerical solution and the analytical solution of subsection 4.2.2 (hereafter referred to as the iω-solution) are compared in Figs. 8 and 9 for $R_c = 100$, $Le = 10$, $N = 1.1$ and $A = 6$. These values are such that the analytical solution given in subsection 4.2.1. (hereafter referred to as the Ω-solution) is nonexistent since the solution to equations (27) and (28) leads to an imaginary value for Ω. The agreement between the two solutions is good except for in the end regions at the top and the bottom of the cavity, see Fig. 8. This is to be expected since the analytical solution is valid only outside these end regions. Note that the solutal end regions in Fig. 8(a), despite the lower diffusivity of solute compared to that of heat, are thicker than their thermal counterparts in Fig. 8(b). This conclusion is in agreement with the results of ref. [6] while at variance with those of ref. [4]. Note also that in spite of the rather large value of R_c, the horizontal profiles of concentration, temperature and velocity in Fig. 9 are not of boundary layer type, and therefore an approximate mathematical analysis based on boundary layer assumption cannot possibly disclose these profiles. It should be remarked that while the Ω-solution can have boundary layer character for sufficiently large R_c, see ref. [6], the iω-solution cannot be of boundary layer type regardless of the value of R_c.

The variations of the numerically computed Sherwood and Nusselt numbers vs N, and comparisons with the analytical solutions, are illustrated in Fig. 10. Extensive numerical investigations of the solutions to equations (27) and (28) and equations (35) and (36) show that for given values of R_c and Le, there exists

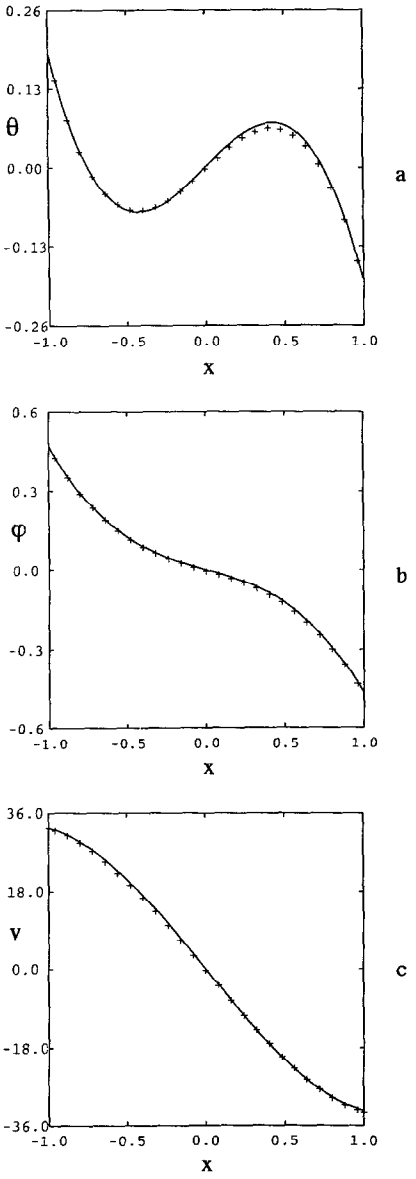

FIG. 9. Comparison between the fully numerical (+) and the analytical (iω) solutions (———) for $R_c = 100$, $Le = 10$, $N = 1.1$, $A = 6$ and $y = 0$, (a) concentration profile, (b) temperature profile, and (c) velocity profile.

a domain $N_\pi(R_c, Le) \leqslant N \leqslant 1$ where one can obtain two physically plausible (i.e. $S_c - NS_T < 0$) analytical solutions: one Ω-solution and one iω-solution. The value of N_π proves to be such that for $N = N_\pi$, ω becomes approximately equal to π. For $N > 1$ the analytical solution is unique and represented by the iω-solution if

$$1 < N < 1 + \left(\frac{15}{2}\right)^{1/3} \left(\frac{Le}{R_c}\right)^{2/3}$$

and by the solution in subsection 4.2.3 if

$$N = 1 + \left(\frac{15}{2}\right)^{1/3} \left(\frac{Le}{R_c}\right)^{2/3}$$

and by the Ω-solution if

$$N > 1 + \left(\frac{15}{2}\right)^{1/3} \left(\frac{Le}{R_c}\right)^{2/3}.$$

In Fig. 10(a), for clarity, only the Ω-solution is plotted for $N \leqslant 1$. In Fig. 10(b), the iω-solution is given in its whole domain of validity together with the Ω-solution where it exists. Fig. 10(a) shows that the analytical and the numerical solutions agree well. From Fig. 10(b) one can conclude that for $N < N_{min}$ the steady-state numerical solution agrees with the Ω-solution while for

$$N_{max} < N < 1 + \left(\frac{15}{2}\right)^{1/3} \left(\frac{Le}{R_c}\right)^{2/3}$$

it agrees with the iω-solution. This conclusion is valid for the high aspect ratio cases, and will be slightly modified in the next subsection. According to Fig. 10(b), a substantial part of the domain $N_\pi(R_c, Le) \leqslant N \leqslant 1$ is covered by the oscillating solution.

5.2. The influence of aspect ratio—the case of intermediate aspect ratios ($1 \leqslant A < 2.5$)

The oscillating solutions discussed in the previous subsection are high aspect ratio phenomena that do not occur for low and intermediate values of the aspect ratio. In other words, for sufficiently large R_c and Le,

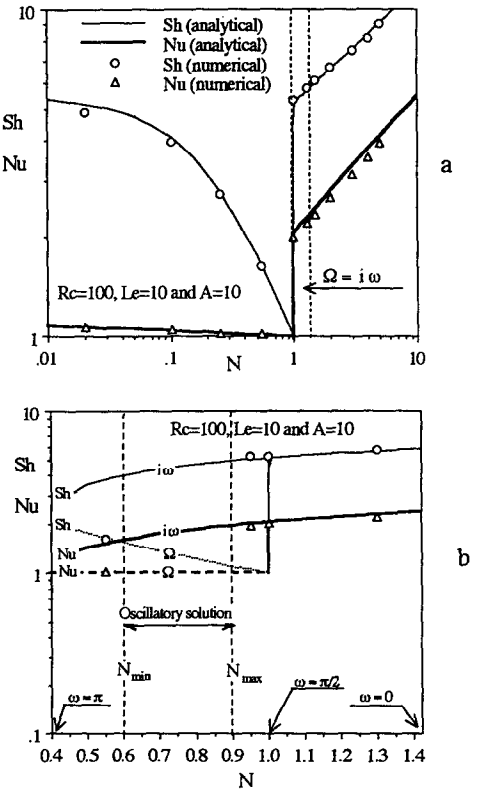

FIG. 10. Comparison between the fully numerically and the analytically computed Sherwood and Nusselt numbers.

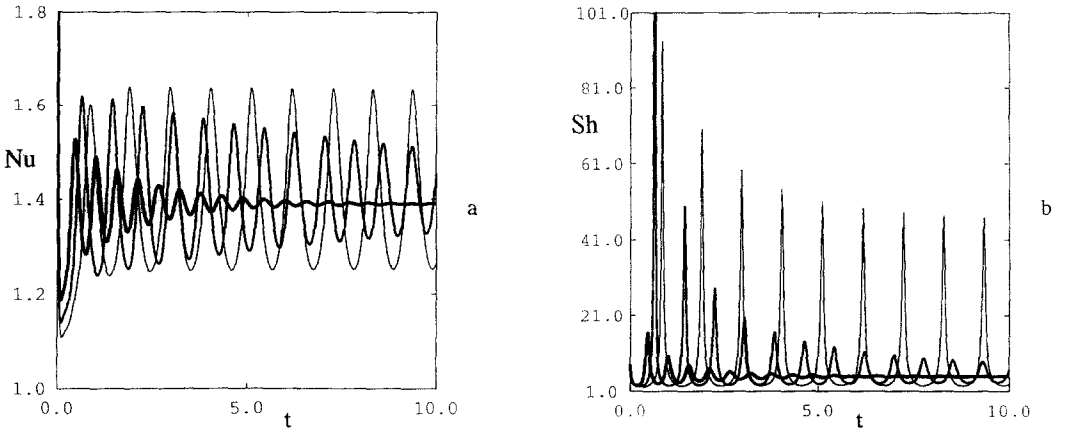

FIG. 11. $R_c = 50$, $Le = 10$, $N = 0.8$, $A = 2$ (thickest line), $A = 3$ and $A = 4$ (thinnest line), (a) Nusselt number vs time, and (b) Sherwood number vs time.

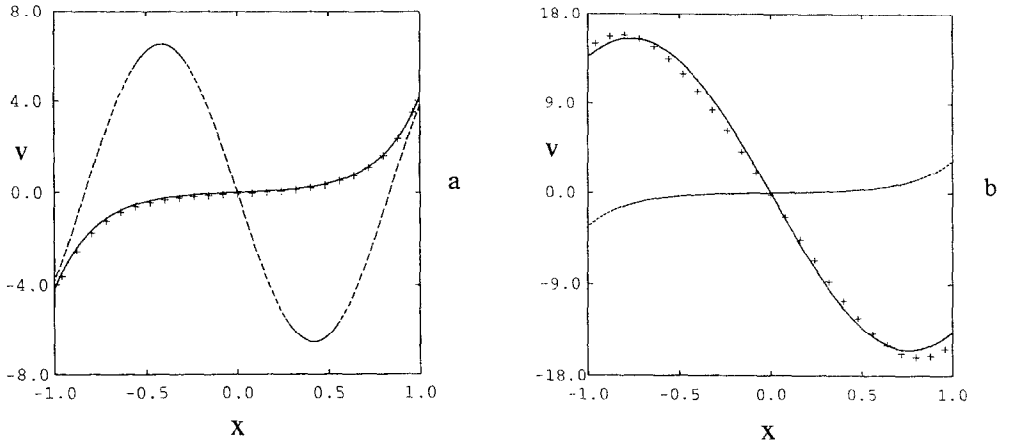

FIG. 12. Comparison between the numerically (+) and the analytically computed velocity profiles for $R_c = 50$, $Le = 10$, $A = 2$ and $y = 0$, (a) $N = 0.6$, and (b) $N = 0.7$. The solid lines represent the Ω-solution in (a) and the $i\omega$-solution in (b), and the dashed lines vice-versa.

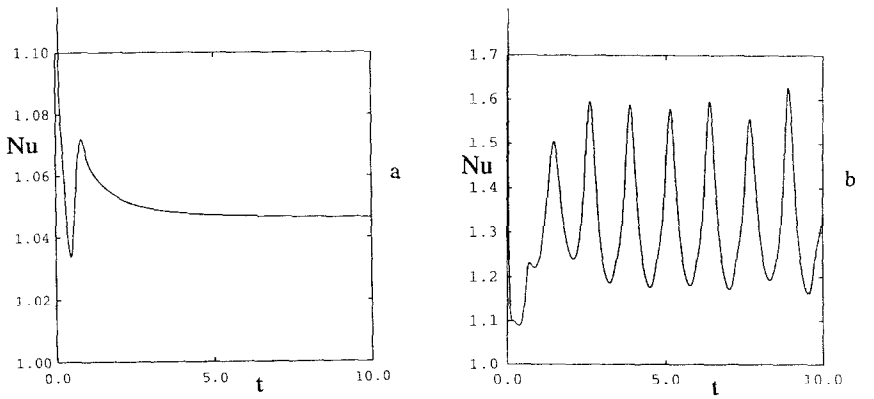

FIG. 13. Nusselt number vs time for $R_c = 50$, $Le = 10$ and $A = 4$, (a) $N = 0.6$, and (b) $N = 0.7$.

there exists a minimum A_{min} ($A_{min} \sim 2$–3 in this paper) such that for $A > A_{min}$ one obtains an oscillating solution if N is in a certain interval ($N_{min} \leqslant N \leqslant N_{max}$) while for $A < A_{min}$ the solution tends to steady state for all values of N. This observation is demonstrated in Fig. 11, according to which, for $R_c = 50$, $N = 0.8$ and $Le = 10$, one obtains an oscillating solution if $A = 4$, whereas decreasing the aspect ratio to $A = 2$ yields a solution that fast approaches steady state.

The properties of the solution, and the influence of A on it, for values of N that are near to N_{min} prove to be interesting. For the cases shown in Figs. 12–14 one can numerically obtain $N_{min} \approx 0.65$ if the aspect ratio is sufficiently large ($A_{min} \sim 3$). Figure 12 shows the numerically and the analytically determined velocity profiles in the cases of $N = 0.6$ ($< N_{min}$) and $N = 0.7$ ($> N_{min}$) for $A = 2$. These parameter values yield two analytical solutions both of which are plotted in Figs. 12(a) and (b). Figure 12(a) shows that for $N = 0.6$, (i) the numerical solution agrees with the Ω-solution, and (ii) the fluid flow direction is counter-clockwise, suggesting that, though of comparable orders of magnitude, the horizontal solutal gradients finally overcome their thermal counterparts. Figure 12(b) on the other hand shows that for $N = 0.7$, which is only slightly larger than 0.6, (i) the numerical solution agrees with the iω-solution, and (ii) the fluid flow direction is clockwise, indicating that, though still of comparable orders of magnitude, the horizontal thermal gradients overcome their solutal counterparts at last. In the present analysis, the profile of velocity at a horizontal cross-section outside the end regions has the same form as the profile of density at that cross-section, i.e. $v \sim \vartheta_c - N\vartheta_T$. Interpreting the velocity profiles shown in Figs. 12(a) and (b) as density profiles, one may conclude that the horizontal gradient of density in the bulk of the enclosure as predicted by the iω-solution is much larger than that predicted by the Ω-solution. The idea discussed earlier that oscillating convection is caused by the destablizing effects of the horizontal gradients of density can now be lent further support in Figs. 13(a) and (b), according to which increasing the aspect ratio to 4, and keeping the other parameter values the same as in Fig. 12, leads to a steady state solution for $N = 0.6$ while it yields an oscillating solution for $N = 0.7$. In Fig. 14, the numerical and analytical solutions are compared in the interval for which the iω- and Ω-solutions exist simultaneously. The main conclusions that can be drawn from Fig. 14 are that (i) for a value of N which is slightly less than N_{min}, transition occurs from counter-clockwise flow, with unstable thermal stratification (corresponding to the Ω-solution), to clockwise flow, with stable thermal stratification (corresponding to the iω-solution), (ii) the aforementioned transition occurs earlier for the lower aspect ratio, and (iii) the oscillating solution is contained in the range of N for which the iω-solution is valid for sufficiently small A.

Our investigation of the transition from unstable to stable thermal stratification and the properties of the oscillating solution reported in this paper has not been exhaustive. Further comprehensive numerical and analytical, not to mention experimental, work remains to be done in order to explain and gain deeper insight into these phenomena.

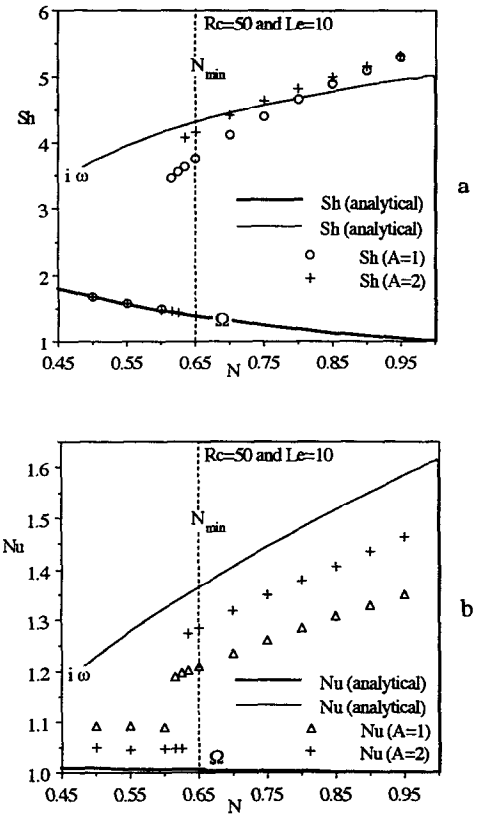

FIG. 14. Comparison between the fully numerically and the analytically computed Sherwood and Nusselt numbers.

Acknowledgement—The first author would like to hereby thank Dr Tetsuo Kimura, the general director of GIRIT, Dr Jun Ikeuchi, the chief of the Department of Metal and Machinery at GIRIT, and the other researchers and employees of GIRIT for the hospitality they showed during the time he stayed at GIRIT as a post-doctoral fellow. Also, Professors Fritz H. Bark, Takeo Sakurai and Ioan Pop are gratefully acknowledged for the many fruitful discussions FA has had with them on the contents of this paper.

REFERENCES

1. D. A. Nield and A. Bejan, *Convection in Porous Media*, pp. 277–303. Springer, New York (1992).
2. D. J. Tritton, *Physical Fluid Dynamics*, pp. 378–392. Oxford University Press, New York (1988).
3. R. W. Griffiths, Layered double-diffusive convection in porous media, *J. Fluid Mech.* **102**, 221–248 (1981).
4. O. V. Trevisan and A. Bejan, Mass and heat transfer by natural convection in a vertical slot filled with porous medium, *Int. J. Heat Mass Transfer* **29**, 403–415 (1986).
5. A. Bejan, The boundary layer regime in a porous layer with uniform heat flux from the side, *Int. J. Heat Mass Transfer* **26**, 1339–1346 (1983).

6. F. Alavyoon, On natural convection in vertical porous enclosures due to prescribed fluxes of heat and mass at the vertical boundaries, *Int. J. Heat Mass Transfer* **36,** 2479–2498 (1993).
7. J. P. Caltagirone, Thermoconvective instabilities in a horizontal porous layer, *J. Fluid Mech.* **72,** 269–287 (1975).
8. S. Kimura, G. Schubert and J. M. Strauss, Route to chaos in porous medium thermal convection, *J. Fluid Mech.* **166,** 305–324 (1986).
9. D. A. Nield, Onset of thermohaline convection in a porous medium, *Water Resour. Res.* **4**(13), 553–560 (1968).
10. N. D. Rosenberg and F. J. Spera, Thermohaline convection in a porous medium heated from below, *Int. J. Heat Mass Transfer* **35,** 1261–1273 (1992).
11. C. Falin and C. F. Chen, Double-diffusive fingering convection in a porous medium, *Int. J. Heat Mass Transfer* **36,** 793–807 (1993).
12. O. V. Trevisan and A. Bejan, Combined heat and mass transfer by natural convection in a porous medium, *Adv. Heat Transfer* **20,** 315–352 (1990).
13. F. Alavyoon and Y. Masuda, Free convection in vertical porous enclosures due to opposing fluxes of heat and solute at the vertical boundaries, *Proceedings of the 6th Symposium of Transport Phenomena*, Seoul (May 1993).